- 1 Low-pressure-temperature stability of pyrope + quartz relative to orthopyroxene + kyanite:
- 2 a new model for aluminous orthopyroxene with vacancies
- 3 Nanfei Cheng^{1*} · David M. Jenkins¹ · Timothy J. B. Holland²
- 4 Department of Geological Sciences and Environmental Studies, Binghamton University,
- 5 Binghamton, NY 13902-6000, USA

8

- 6 ² Department of Earth Sciences, University of Cambridge, Cambridge, CB2 3EQ, UK
- * Corresponding author: Telephone +1 (607) 7592770. Email: ncheng5@binghamton.edu

10 Abstract

Determination of the stability of pyrope with quartz could provide theoretical pressure-
temperature (P-T) constraints on silica-saturated eclogites as well as near end-member pyrope-
bearing terrains. The lower-P-T stability of pyrope in the presence of quartz in the system MgO-
Al_2O_3 -SiO ₂ can be modeled by the reaction: 3 enstatite + 2 kyanite = 2 pyrope + 2 quartz.
Reaction reversals were experimentally obtained using a ½-inch diameter piston-cylinder press
and a 1000-ton multi-anvil press. Besides natural quartz, all other starting materials, including
orthopyroxene, pyrope, and kyanite, were synthesized. The reaction has been bracketed at 1.50
GPa at 1040–1080 °C; 1.69–1.79 GPa at 1000 °C; 2.26 GPa at 920–940 °C; 2.90 GPa at 840–
860 °C. The bracketed boundary is higher in temperature and pressure than that calculated using
the newest dataset of Holland et al. (2018), particularly at higher pressures. Aluminum is usually
thought to be taken into orthopyroxene in the form of Mg-tschermak's pyroxene (MgTs;
MgAl ₂ SiO ₆) under these experimental <i>P-T</i> conditions. In contrast, the observed orthopyroxene
composition indicated the involvement of a non-stoichiometric component Mg-eskola pyroxene
(MgEs; $Mg_{0.5}\square_{0.5}AlSi_2O_6$), an aluminous orthopyroxene with octahedral vacancies (\square). End-
member thermodynamic properties for MgEs as well as a mixing model for the ternary enstatite-
MgTs-MgEs solid solution have been derived. The thermodynamic calculations, employing the
mixing model, are in good agreement with the experimental brackets. The new model has
potential applications to constrain <i>P-T</i> conditions of tectonic settings such as ultrahigh pressure
and ultrahigh temperature metamorphism.
Keywords: orthopyroxene · quartz · pyrope · non-stoichiometry · Mg-eskola pyroxene · Mg-
tschermak's pyroxene

33 Introduction

Pyrope (Mg₃Al₂Si₃O₁₂) is an important component in garnet. Determining the lower-pressure-temperature (*P-T*) stability of pyrope in the presence of quartz helps constrain the stability of quartz-bearing eclogites and therefore the depths to which crustal rocks in high pressure/ultrahigh pressure (HP/UHP) terranes can be transferred. It also defines the lower-temperature stability of the nearly pure pyrope-bearing quartzites of the Dora Maira massif of the Western Alps (e.g., Chopin 1984).

The *P-T* stability of pyrope in the absence of quartz has been well studied most recently by Fockenberg (2008). Aside from the approximate boundary proposed by Hensen and Essene (1971) and Hensen (1972), however, there has been no detailed study of the lower *P-T* stability of pyrope in the presence of quartz.

In the chemical system $MgO-Al_2O_3-SiO_2$ (MAS), the lower-P-T stability of pyrope with quartz is defined by the reaction:

$$46 3 Mg2Si2O6 + 2 Al2SiO5 = 2 Mg3Al2Si3O12 + 2 SiO2 (1)$$

47 orthopyroxene kyanite pyrope quartz

Critical for the location of this reaction is the Al_2O_3 content in orthopyroxene (Opx). The solubility of Al_2O_3 in orthopyroxene has long been of interest to petrologists for its potential application to geothermobarometry. Accordingly, experimental investigations of alumina in orthopyroxene as a function of P-T conditions and bulk compositions have been conducted over decades (e.g., Boyd and England 1964; MacGregor 1974; Herzberg 1983; Aranovich and Berman 1997; Hollis and Harley 2003; and references therein). In these studies, a common assumption is that Al_2O_3 is taken into orthopyroxene in the form of Mg-tschermak's pyroxene (Mg $Al_2SiO_6 = MgTs$), and aluminous orthopyroxene is usually described as a binary enstatite—

56 MgTs solid solution. The assumption appears reliable in silica-deficit systems such as in spinel 57 and garnet peridotites (e.g., Danckwerth and Newton 1978; Perkins et al. 1981; Gasparik and Newton 1984). However, a nonstoichiometric component Mg-eskola pyroxene 58 $(Mg_{0.5}\square_{0.5}AlSi_2O_6 = MgEs$, where \square represents a vacancy) is predicted to be present in silica-59 rich systems (Boyd and England 1960; Gasparik 1994; Fockenberg and Schrever 1997). 60 Eskola (1921) introduced the terminology "pseudojadeite" to describe nonstoichiometric 61 62 molecules of pyroxene when documenting the eclogites of Norway (Day and Mulcahy 2007; Kawasaki and Osanai 2015). Unlike the analogous nonstoichiometric Ca-eskola pyroxene (CaEs; 63 $Ca_{0.5}\square_{0.5}AlSi_2O_6$), which has been well investigated (e.g., Schroeder-Frerkes et al. 2016; and 64 references therein), the nonstoichiometric Mg-eskola orthopyroxene has rarely been addressed. 65 Boyd and England (1960) observed the variation in Mg/Si ratio and deviation of the 66 orthopyroxene composition from the enstatite-pyrope join to the direction of an excess of SiO₂, 67 68 and related the variation to the saturation of silica in the environment. Sekine and Wyllie (1983) 69 also noted that aluminous orthopyroxene coexisting with SiO₂-rich liquids appeared to have excess SiO₂ and deviated from the enstatite-MgTs join. Fockenberg and Schreyer (1997) 70 71 synthesized excess-Si aluminous orthopyroxene in the system MAS with gels as the starting 72 materials. The Mg-deficiencies and Si-excess were supported by mineral compositions and cell dimensions, while transmission electron microscopy confirmed the anhydrous nature of the 73 74 orthopyroxene. In light of these studies a new model is needed for aluminous orthopyroxene. involving MgEs substitution as well as MgTs substitution. 75 76 A failure to include MgEs for aluminous orthopyroxene in a silica-rich system would

result in systematic errors in Al_2O_3 isopleths of orthopyroxene and in deduced P-T conditions

(e.g., Arima and Onuma 1977; Baba 1999; Hollis and Harley 2003), particularly at high pressures.

In this study, these deficiencies are remedied by direct experimental reversal of reaction (1) in the range of 740–1100 °C and 1.5–3.3 GPa using piston-cylinder and multi-anvil presses. The experimental results are compared with the calculated reaction boundary using the existing dataset of Holland et al. (2018). Evidence for variation in MgEs component in mineral composition and unit-cell parameters is also presented before proposing a new mixing model for aluminous orthopyroxene and discussing its potential applications to tectonic settings.

Experimental methods

Starting materials

Besides natural quartz, the phases pyrope, Opx, and kyanite in the starting mixtures were synthesized from appropriate mixtures of reagent-grade SiO₂, Al₂O₃ (Aldrich, lot no. 2121CL), and MgO (Aldrich, lot no. 05225DR) or Mg(OH)₂ (Alfa Aesar, lot no. G07X026). The SiO₂ was made from silicic acid (J.T. Baker, lot no. 926407) heated overnight in air to 1100 °C, producing amorphous silica or weakly crystalline cristobalite (Jenkins 2011). Although all these minerals are anhydrous, water was added in the form of distilled water or from the breakdown of Mg(OH)₂ as a flux improving the reaction rate during synthesis. After weighing according to stoichiometry, reagents were mixed thoroughly under acetone in an agate mortar. The detailed conditions and products of synthesis are listed in Table 1.

Three kinds of starting mixtures were prepared for reaction reversal experiments. All mixtures had the same assemblage of phases (pyrope, quartz, Opx, and kyanite) but with different Opx starting compositions: Al-free, medium-Al, and high-Al Opx. Each sample was

prepared by sealing \sim 6 mg of the starting mixture in a platinum (Pt) capsule along with 1–3 wt% water to guarantee appreciable reaction while avoiding the total dissolution of quartz. The water was added into the capsule using a syringe and finally reached the desired amount by evaporation on a Mettler-Toledo AG245 balance which has a precision of \pm 0.02 mg.

Apparatus and methods

Experiments below 2.5 GPa were conducted in a non-end-loaded ½-inch diameter piston-cylinder press with NaCl/pyrex as pressure media. The accuracy of pressure measurement is estimated to be \pm 0.05 GPa. The K-type chromel-alumel thermocouple was used to measure temperature. The uncertainties are estimated to be \pm 5 °C for reversed runs using 1.5 mm outer diameter (OD) Pt capsules and \pm 10°C for mineral synthesis runs using 4.0 or 5.0 mm OD Pt capsules (e.g., Jenkins 2011).

In consideration of the relatively high temperature of this study, a double-sleeve NaCl/pyrex (Fig. 1a), instead of a single-sleeve NaCl, pressure cell was adopted. Pressure correction for the NaCl/pyrex media was made against the experimentally determined boundary of 2 ferrosilite = fayalite + quartz at 1000 °C. Synthetic ferrosilite and fayalite along with natural quartz were used as starting materials. The boundary of nominal pressure was bracketed between 1.49 and 1.51 GPa (Fig. 1b), which indicated a friction correction of -6% compared to 1.41 GPa as determined by Bohlen et al. (1980).

Experiments above 2.5 GPa were performed in a 1000-ton multi-anvil press with 18/11 mm octahedra made of castable MgO pressure media (Walker et al. 1990). A recalibration for pressure was done at 830 °C (Cheng et al. under review) against reaction boundaries of quartz = coesite (Bose and Ganguly 1995) and albite = jadeite + quartz (Holland 1980). K-type thermocouples were used to measure temperature. A pressure uncertainty of \pm 0.1 GPa and a

temperature uncertainty of \pm 10 °C were adopted (Corona et al. 2013). Pt Capsules with 1.5 mm OD and \sim 6 mm length were used.

Analytical methods

124

125

126

127

128

129

130

131

132

133

134

135

136

137

138

139

140

141

142

143

144

145

146

Powder X-ray diffraction (XRD) patterns were measured on a Panalytical PW3040-MPD X-ray diffractometer. Operating conditions were 40 kV and 20 mA using Cu Kα radiation with a graphite diffracted-beam monochromator. All run products were mounted on a zero-background oriented quartz plate as a thin smear and scanned over the range of 5-60 °20 with a step size of $0.05 \, ^{\circ}2\Theta$ and counting times of one second per step. Rietveld refinements were obtained using the GSAS-EXPGUI package (Toby 2001; Larson and Von Dreele 2004) to make quantitative phase analysis and to measure unit-cell parameters. Rietveld refinements were initiated using the structures of pyrope (*Ia3d*) from Novak and Gibbs (1971), quartz (*P*3₂21) from Levien et al. (1980), enstatite (*Pbca*) from Nestola et al. (2006), and kyanite ($P\overline{1}$) from Comodi et al. (1997). Convergence criterion was set to 0.03. The background was modeled using the shifted Chebyschev (function 1) with 6 terms. The profile peak cutoff was 0.002 with the default function 2. The zeropoint was refined against quartz ($a_0 = 4.9139 \text{ Å}$, $c_0 = 5.40595 \text{ Å}$), used as an internal standard for the other phases. A preferred orientation 610 plane was refined for Al-free and medium-Al Opx. Unit-cell parameters for the synthetic phases are listed in Table 2. Run products, with different starting Opx, near the reaction boundary and at the stability field of Opx and kyanite were prepared for electron microprobe analysis. Samples were mounted in epoxy and polished with diamond grit in steps down to 0.5 µm (Jenkins and Corona 2006). The analysis of individual Opx was done on a JEOL 8900 Superprobe operated at 15 kV and 10 nA. Semi-quantitative EDS (energy dispersive X-ray spectroscopy) analysis was done before selecting points for quantitative WDS (wavelength dispersive spectroscopy) analysis.

Experimental results

Reaction boundary

Reaction directions were assessed by comparing powder XRD patterns of run products with the starting materials and calculating weight percent of phases using Rietveld refinement. Only runs with appreciable changes in main XRD peak heights were accepted. Table 3 lists the experimental conditions and products while Fig. 2 shows the results in *P-T* space. Because the reaction rate was low and the amount of kyanite and quartz could change due to the change of composition of orthopyroxene, only changes in proportions of the dominant phases orthopyroxene and pyrope were adopted as the main criterion to determine the reaction direction. The reaction was bracketed at 1.50 GPa at 1040–1080 °C; 1.69–1.79 GPa at 1000 °C; 2.26 GPa at 920–940 °C; 2.90 GPa at 840–860 °C; and with coesite half-bracketed at 3.30 GPa at 780 °C because the nucleation of talc interfered with the growth of orthopyroxene at lower temperatures. These results are lower in pressure than the uncorrected "piston out" reversal bracket of Hensen (1972) (Fig. 2).

Compositional reversals in the Al₂O₃ contents of orthopyroxene

Experimental reversals of the Al_2O_3 contents of orthopyroxene were determined with two or three kinds of starting orthopyroxene: Al-free, high-Al, and medium-Al. As shown in Fig. 3, there is a range in Al_2O_3 contents, indicating lack of complete equilibration. The equilibrium contents were estimated from the overlap in the re-equilibrated run products conducted at the same condition near the reaction boundary. The population of Al_2O_3 contents was also used to narrow the estimation. The approach gives an estimation of Al_2O_3 contents in orthopyroxene of 12.5 ± 1.5 wt% at 1.50 GPa and 1060 °C, $\sim 10.5 \pm 1.0$ wt% at 1.69 GPa and 1000 °C, $\sim 7.2 \pm 1.2$

wt% at 2.26 GPa and 920 °C, and \sim 6.0 \pm 1.0 wt% at 2.90 GPa and 840 °C. This is the first study to report composition data for this reaction.

173 Discussion

Thermodynamic modeling with the current model for aluminous Opx

A thermodynamic calculation was done to model this reaction employing the program THERMOCALC v3.45 (Powell et al. 1998) and the latest version (ds633, Holland et al. 2018) of the thermodynamic dataset of Holland and Powell (2011). Aluminum is usually assumed to be taken into orthopyroxene in the form of Mg-tschermak's molecule under these experimental *P-T* conditions. Therefore, a mixing model for the binary enstatite-MgTs solid solution was initially adopted. The modeled results turn out to be good at lower pressures but fail to fit the experimental brackets at higher pressures (Fig. 2). If this is due to omission of an Mg-eskola substitution, then it may suggest a need to improve the mixing model of aluminous orthopyroxene.

Non-stoichiometric pyroxene

Stoichiometry is usually a criterion used to evaluate and accept data for mineral composition analysis (e.g., Hensen and Essene 1971; Lee and Ganguly 1988). However, it may mistakenly exclude the presence of non-stoichiometric components which occupy fewer cations than stoichiometric components. Plotting all data of orthopyroxene composition of this study on a ternary En-MgTs-MgEs diagram indicates that most pyroxenes show some departure from stoichiometric En-MgTs join towards the non-stoichiometric (vacancy-bearing) MgEs (Fig. 4). Opx involves increasing ratio of MgEs/MgTs with the increase of pressure. This may be accounted for by introducing the MgEs (Mg-eskola pyroxene, Mg_{0.5} $\square_{0.5}$ AlSi₂O₆) substitution as

well as the well-known MgTs (Mg-tschermak's pyroxene, MgAl₂SiO₆) substitution for En (enstatite, Mg₂Si₂O₆). The nonstoichiometric molecule may enhance the stability of the aluminous orthopyroxenes. This requires derivation of end-member thermodynamic properties for MgEs as well as a mixing model for the ternary En–MgTs–MgEs solid solution.

Estimation of molar volume of MgEs

Before setting up a new mixing model, the molar volume of MgEs was estimated from the mineral composition and unit-cell volumes of this study (Table 5) as well as from the data of Fockenberg and Schreyer (1997). Because the composition of orthopyroxene is not homogeneous in this study, the average values of ~40 analyses for each run product were adopted to obtain an estimation of aluminum content per six oxygen atoms and the molar fractions of the three end members. The unit-cell parameters of orthopyroxene were determined from Rietveld refinements of the powder XRD patterns. The volume was presumed to be additive according to the equation:

$$V_{\text{Opx}} = V_{\text{En}} X_{\text{En}} + V_{\text{MgTs}} X_{\text{MgTs}} + V_{\text{MgEs}} X_{\text{MgEs}}$$

where V_i represents molar volume and X_i molar fraction of component i.

Thus, a linear relationship between X_{MgEs} and $V_{MgEs}X_{MgEs}$ could be derived.

$$y = ax$$

where:

209
$$y = V_{\text{MgEs}} X_{\text{MgEs}} = V_{\text{Opx}} - V_{\text{En}} X_{\text{En}} - V_{\text{MgTs}} X_{\text{MgTs}}$$

$$x = X_{\text{MgEs}}$$

$$a = V_{\text{MgEs}}$$

The slope should be V_{MgEs} , the molar volume of MgEs. Using volumes of En and MgTs from

Holland and Powell (2011) and letting the line go through the origin, the linear fitting of y = axgave a value of 5.927 ± 0.111 J/bar for V_{MgEs} (Fig. 5).

New model for aluminous orthopyroxene with vacancies

213

214

215

216

The ternary En–MgTs–MgEs solid solution may be described by extending the simple En–MgTs mixing model, using the three end-members whose structural formulae are, with \Box denoting a vacancy:

Component	Site					
	M2	M1	Т			
En	Mg	Mg	Si ₂			
MgTs	Mg	Al	AlSi			
MgEs	$\square_{\frac{1}{2}}Mg_{\frac{1}{2}}$	Al	Si ₂			

Mixing is described in terms of ideal mixing on the octahedral (M2, M1) and tetrahedral (T) sites for configurational entropy and a regular solution to describe departures from ideality. The site fractions, in terms of two compositional variables $y = x_{AlM1}$, mole fraction of Al in the M1) and $z = 2x_{\square,M2}$ are

$$x_{\square,M2} = z/2$$
 $x_{MgM2} = 1 - z/2$ $x_{AlM1} = y$ $x_{MgM1} = 1 - y$ $x_{SiT} = 1 - y/2 + z/2$

and end-member proportions given by

$$p_{\rm En} = 1 - y$$
 $p_{\rm MgTs} = y - z$
 $p_{\rm MgEs} = z$

The ideal activities are expressed as

$$a_{\text{En}} = x_{\text{MgM2}} x_{\text{MgM1}} (x_{\text{SiT}})^{\frac{1}{2}}$$

$$a_{\text{MgTs}} = \frac{1}{\sqrt{\frac{1}{2}}} x_{\text{MgM2}} x_{\text{AlM1}} (x_{\text{AlT}})^{\frac{1}{4}} (x_{\text{SiT}})^{\frac{1}{4}}$$

$$a_{\text{MgEs}} = 2 (x_{\text{DM2}})^{\frac{1}{2}} (x_{\text{MgM2}})^{\frac{1}{2}} x_{\text{AlM1}} (x_{\text{SiT}})^{\frac{1}{2}}$$

The T-site terms have been additionally raised to the power of $\frac{1}{4}$ to impose a quarter of the usual entropy of mixing to accommodate for short-range ordering on the tetrahedral and octahedral sites. It was found (Holland and Powell, 2011) that complete Al-Si disorder does not allow fitting of aluminous opx compositions in the many MAS system equilibria considered, whereas reduction to $\frac{1}{4}$ of configurational entropy satisfied the experiments well. The non-ideal mixing is taken as a regular solution of the 3 end-members, with values

$$w_{\text{En,MgTs}} = 18.5 - 0.12P \text{ (kJ)}$$

 $w_{\text{En,MgEs}} = 14.5 - 0.17P \text{ (kJ)}$
 $w_{\text{MgTs,MgEs}} = -15.0 \text{ (kJ)}$

The thermodynamic properties of the MgEs end-member and w values were determined by fitting the experimental data for the reaction 3 enstatite + 2 kyanite = 2 pyrope + 2 quartz along with several other MAS equilibria by monte-carlo optimisation. The molar volume of the MgEs end-member used here (5.927 J/bar) is derived from cell volume data presented as above. All other components to the Gibbs energy of MgEs were determined from a summation approximation ($G_{\text{MgEs}} = \frac{1}{2}G_{\text{MgTs}} + \frac{3}{2}G_{\text{En}} - \frac{3}{2}G_{\text{Fo}}$). Although, in principle, the parameters could be derived solely from the experiments of this study, the allocation of Al to two different pyroxene substitutions requires modification of the MgTs end-member enthalpy of formation relative to the Holland & Powell (2011) dataset. The set of equilibria used in fitting was pyrope Opx quartz kyanite (This study)

240 forsterite (Fo) pyrope spinel Opx (Danckwerth and Newton 1978; Gasparik and Newton 1984)

Opx spinel forsterite (Gasparik and Newton 1984)

242 Opx pyrope (Perkins et al. 1981)

243 cordierite + quartz + Opx + sillimanite (Newton, pers comm, in Holland and Powell 2011)

and this assures compatibility with the tc-ds633 dataset of Holland et al. (2018). Results from the

monte-carlo fitting indicated that silica-deficient assemblages (those with spinel, forsterite,

sapphirine) have very little MgEs component while those coexisting with quartz contain

significant amounts.

The mixing properties ($w_{\rm En,MgTs}$, $w_{\rm En,MgEs}$) were quite closely constrained by the equilibria involved, with $w_{\rm En,MgTs}$ being a little larger than in the earlier models so as to accommodate more MgEs and less MgTs component in pyroxenes. The value for $w_{\rm MgTs,MgEs}$ was less well constrained and was set to -15 kJ, the same as the analogous $w_{\rm CaTs,CaEs}$ (Holland and Powell 2011). The enthalpy of formation of MgTs needed adjusting by -2.25 kJ relative to the dataset value, and the new MgEs end-member required adjusting by 35.0 kJ relative to the sum $\frac{1}{2}$ MgTs $+\frac{3}{2}$ En $-\frac{3}{2}$ Fo.

As can be seen in Fig. 6, the revised calculated curve is in greater agreement with the experimental brackets.

The composition of the pyroxenes may be found from the THERMOCALC output, as shown in Appendix 1, where the values for $x_{\rm MgTs} = y - z$ and $x_{\rm MgEs} = z$ are given as output and the total Al (pfu) is Al = 2y - z. Comparing these with the experimental results, the agreement is good at high temperatures, but calculated Al contents are much lower at 800–900°C. This may be due to sluggish diffusion at lower temperatures which prevents the alumina content from

reaching the equilibrium compositions, but further investigation is needed to understand this inconsistency between the calculated and observed Al_2O_3 contents at lower temperatures.

Implications for Opx in silica-rich systems

262

263

264

265

266

267

268

269

270

271

272

273

274

275

276

277

278

279

280

281

282

283

284

(1) UHP whiteschist from the Dora-Maira Massif

The Dora-Maira Massif is well-known for being the first record of coesite in a metamorphic terrane, indicating UHP conditions, in the pyrope-coesite rocks reported by Chopin (1984). There were several approaches used to estimate the peak metamorphic P-T condition of Dora-Maira Massif. Chopin and Schertl (1999) constrained the peak metamorphism to 3.7 GPa and 790 °C by combining the garnet-clinopyroxene-phengite geobarometer with the garnetclinopyroxene geothermometer for the UHP eclogite, while Nakamura and Banno (1997) gave an estimation of P-T from 3.3 GPa and 760 °C to 3.4 GPa and 830 °C for the eclogite using a garnet-omphacite-kyanite-coesite geothermobarometer. But a problem for those geothermometers is the estimation of Fe³⁺/Fe²⁺ of pyroxenes which is usually based on mineral stoichiometry. At such *P-T* conditions, there should be a significant quantity of nonstoichiometric end members, such as CaEs, in the clinopyroxene. Thus, estimation of Fe³⁺/Fe²⁺ by stoichiometry can be highly problematic and could produce non-negligible errors for P-T estimation (Proyer et al. 2004). Another important approach is the combination of Si-inphengite barometry with the dehydration reaction from talc + kyanite to pyrope + coesite + H₂O (Chopin 1985; Massonne and Schreyer 1989; Schertl et al. 1991). However, dissolved solutes in the fluid could change the activity of $H_2O(a_{H_2O})$ and thus shift the reaction boundary to lower temperatures. The solutes are usually assumed to be salts (mainly alkali chlorides) and gases (mainly CO₂) at low pressures, but substantial amounts of host-rock oxide components (mainly silicates and aluminosilicates) are also predicted at high pressures (Hermann 2003; Sverjensky et

al. 2014; Manning 2018). Such complex mixtures of solutes make it hard to estimate a_{H_2O} and determine the reaction boundary at UHP conditions. Coggon and Holland (2002) estimated the P-T conditions (3.3 GPa and 721°C) of these rocks using both a pseudosection and multiple-reaction thermobarometry by lowering a_{H_2O} to 0.5 on the basis of stable isotope thermometry (C. Chopin personal communication, in Coggon and Holland 2002). However, their result rests on assuming the a_{H_2O} as 0.5.

Reaction (1) involving coesite, namely the reaction of Opx + kyanite to pyrope + coesite, in the system MAS is water-free and thus knowledge of a_{H_2O} is not needed for applying this reaction to geological settings. The calculated reaction boundary, employing the model of Opx from this study, could provide a minimum estimation of peak metamorphic temperature.

Combination of this reaction with the Si-in-phengite barometer (Si = 3.55; Schertl et al. 1991) gives an estimation of 3.6 GPa and 725 °C (Fig. 7).

The Si-in-phengite barometer for Si = 3.55 gave a lower pressure of 3.3 GPa in the recalibration of Coggon and Holland (2002), partly because the Parigi phengites in the Dora Maira massif contain Ca, Na, Fe, and Ti as well as some A-site vacancies and a small trioctahedral component. Applying this pressure to reaction (1) will give a temperature of 775 °C (Fig. 7), which is higher than the 721 °C value of Coggon and Holland (2002) and indicates the a_{H_2O} could not have been lower than 0.5.

(2) Sapphirine-quartz-Opx assemblage at ultrahigh-temperature conditions

The sapphirine-quartz assemblage is a benchmark criterion for ultrahigh-temperature (UHT) metamorphism which is defined as a subdivision of granulite facies metamorphism with temperature > 900 °C and pressure in the range of 0.7-1.3 GPa (Harley 1998a, 2008; Kelsey 2008; Kelsey and Hand 2015). The aluminous orthopyroxene coexisting with sapphirine + quartz

could give an essential constraint for the peak-temperature estimation because of the relatively sluggish diffusion of Al compared to Fe-Mg exchange during cooling (Aranovich and Podlesskii 1989; Harley 1998b; Hollis and Harley 2003). However, MgTs was assumed to be the only component carrying alumina, which could introduce some undesired errors for the Al-in-Opx thermometer. As shown in Fig. 8, the new model involving MgEs gives more closely-spaced isopleths of Al₂O₃ in orthopyroxene coexisting with sapphirine and quartz in the system MAS. The new model would, for example, result in temperature that are 50 °C (or more) higher in the range of 1100-1200 °C, depending on the Al₂O₃ in orthopyroxene. The ternary En–MgTs–MgEs orthopyroxene model could revise the quantitative *P-T* estimations for UHT metamorphism involving aluminous orthopyroxene and other aluminous phases in a silica-rich system.

319 Conclusion

Reversed experiments were conducted to constrain the lower-P-T stability of pyrope in the presence of quartz in the system MgO–Al $_2$ O $_3$ –SiO $_2$. The reaction, 3 enstatite + 2 kyanite = 2 pyrope + 2 quartz, was also modeled using the thermodynamic data of Holland et al. (2018), which yielded a curve that deviates systematically to lower pressures at lower temperatures compared with the experimental brackets. The finding in this study that the pyroxenes showed departure from stoichiometry towards an excess of silica, along with evidence from previous studies (Sekine and Wyllie 1983; Fockenberg and Schreyer 1997), suggests that the Mg-Eskola substitution may be enhancing the stability of the aluminous enstatites.

The end-member thermodynamic properties for MgEs as well as a mixing model for the ternary En–MgEs solid solution have been derived. The derivation included the data from this study as well as those of many previous experiments in the system MgO–Al₂O₃–SiO₂, thus

assuring compatibility with the tc-ds633 dataset of Holland et al. (2018). The calculated curve is now in quite good agreement with the experimental brackets of this study.

The new model has potential applications to constrain the *P-T* conditions of both UHP whiteschists and UHT pelites. It also calls for the necessity to include MgEs as well as CaEs in pyroxenes in silica-rich systems to achieve better thermodynamic modeling for high-pressure and high-temperature metamorphism.

Acknowledgments

Thanks go to D. Collins for assistance with the electron microprobe analyses. Two anonymous reviewers are greatly acknowledged for their constructive and insightful reviews. T. L. Grove is appreciated for careful editorial handling. This research was supported in part by funding from the NSF grant EAR-1725053 to DMJ.

344 Appendix 1

Compositions of pyroxenes for reaction (1) in the text may be found from the THERMOCALC output, as illustrated below at the indicated P-T conditions. The total Al content is calculated as Al = 2y-z, and the corresponding wt% of Al₂O₃ is given for comparison with the data in Figure 3.

P(kbar)	T(°C)	y(opx)	z(opx)	wt% Al ₂ O ₃
29.6329	841.055	0.06973	0.06722	1.84
28.6847	850.000	0.07066	0.06696	1.89
26.0830	875.000	0.07469	0.06486	2.15
23.6421	900.000	0.08197	0.06056	2.63
21.4642	925.000	0.09325	0.05507	3.34
19.5920	950.000	0.1085	0.04987	4.25
18.0121	975.000	0.1275	0.04567	5.32
16.6471	1000.000	0.1509	0.04234	6.60
15.6410	1025.000	0.1772	0.04094	7.97
14.9691	1050.000	0.2051	0.04138	9.37
14.5566	1075.000	0.2341	0.04325	10.80
14.3518	1100.000	0.2637	0.04633	12.22

351	References
352	Aranovich LY, Berman RG (1997) A new garnet-orthopyroxene thermometer based on reversed
353	Al_2O_3 solubility in FeO- Al_2O_3 -SiO $_2$ orthopyroxene. Am Mineral 82:345–353. doi:
354	10.2138/am-1997-3-413
355	Aranovich LY, Podlesskii KK (1989) Geothermobarometry of high-grade metapelites:
356	simultaneously operating reactions. Geol Soc London, Spec Publ 43:45-61. doi:
357	10.1144/GSL.SP.1989.043.01.03
358	Arima M, Onuma K (1977) The solubility of alumina in enstatite and the phase equilibria in the
359	join MgSiO ₃ -MgAl ₂ SiO ₆ at 10-25 kbar. Contrib Mineral Petrol 61:251–265. doi:
360	10.1007/BF00376700
361	Baba S (1999) Sapphirine-bearing orthopyroxene-kyanite/sillimanite granulites from South
362	Harris, NW Scotland: Evidence for Proterozoic UHT metamorphism in the Lewisian.
363	Contrib Mineral Petrol 136:33-47. doi: 10.1007/s004100050522
364	Bohlen SR, Essene EJ, Boettcher AL (1980) Reinvestigation and application of olivine-quartz-
365	orthopyroxene barometry. Earth Planet Sci Lett 47:1-10. doi: 10.1016/0012-
366	821X(80)90098-9
367	Bose K, Ganguly J (1995) Quartz-coesite transition revisited: reversed experimental
368	determination at 500-1200 °C and retrieved thermochemical properties. Am Mineral
369	80:231–238. doi: 10.2138/am-1995-3-404
370	Boyd FR, England JL (1960) Minerals of the mantle. Carnegie Inst Washingt Yearb 59:47-52
371	Boyd FR, England JL (1964) The system enstatite-pyrope. Carnegie Inst Washingt Yearb
372	63:157–161
373	Chopin C (1984) Coesite and pure pyrope in high-grade blueschists of the Western Alps: a first

374	record and some consequences. Contrib Mineral Petrol 86:107-118. doi:
375	10.1007/BF00381838
376	Chopin C (1985) Les relations de phase dans les métapelites de haute pression. Approche
377	expérimentale et naturaliste, conséquences géodynamiques pour les Alpes occidentales.
378	PhD dissertation, Université Pierre et Marie Curie - Paris VI
379	Chopin C, Schertl H-P (1999) The UHP unit in the Dora-Maira Massif, Western Alps. Int Geol
380	Rev 41:765–780. doi: 10.1080/00206819909465168
381	Coggon R, Holland TJB (2002) Mixing properties of phengitic micas and revised garnet-
382	phengite thermobarometers. J Metamorph Geol 20:683-696. doi: 10.1046/j.1525-
383	1314.2002.00395.x
384	Comodi P, Zanazzi PF, Poli S, Schmidt MW (1997) High-pressure behavior of kyanite:
385	Compressibility and structural deformations. Am Mineral 82:452-459. doi: 10.2138/am-
386	1997-5-602
387	Danckwerth PA, Newton RC (1978) Experimental determination of the spinel peridotite to
388	garnet peridotite reaction in the system MgO-Al $_2$ O $_3$ -SiO $_2$ in the range 900 °-1100 °C and
389	Al ₂ O ₃ isopleths of enstatite in the spinel field. Contrib Mineral Petrol 66:189–201. doi:
390	10.1007/BF00372158
391	Day HW, Mulcahy SR (2007) Excess silica in omphacite and the formation of free silica in
392	eclogite. J Metamorph Geol 25:37–50. doi: 10.1111/j.1525-1314.2006.00677.x
393	Eskola P (1921) On the eclogites of Norway. Vindenskaps Selskapets Skriefter, Klasse
394	Fockenberg T (2008) Pressure–temperature stability of pyrope in the system MgO–Al ₂ O ₃ –SiO ₂
395	H ₂ O. Eur J Mineral 20:735–744. doi: 10.1127/0935-1221/2008/0020-1868
396	Fockenberg T, Schreyer W (1997) Synthesis and chemistry of unusual excess-Si aluminous

397	enstatite in the system MgO-Al ₂ O ₃ -SiO ₂ (MAS). Eur J Mineral 9:509-518. doi:
398	10.1127/ejm/9/3/0509
399	Gasparik T (1994) A petrognetic grid for the system MgO-Al ₂ O ₂ -SiO ₂ . J Geol 102:97–109
400	Gasparik T, Newton RC (1984) The reversed alumina contents of orthopyroxene in equilibrium
401	with spinel and forsterite in the system MgO-Al ₂ O ₃ -SiO ₂ . Contrib Mineral Petrol 85:186–
402	196. doi: 10.1007/BF00371708
403	Hamilton NE, Ferry M (2018) ggtern: Ternary Diagrams Using ggplot2. J Stat Softw 87:. doi:
404	10.18637/jss.v087.c03
405	Harley SL (1998a) On the occurrence and characterization of ultrahigh-temperature crustal
406	metamorphism. Geol Soc London, Spec Publ 138:81-107. doi:
407	10.1144/GSL.SP.1996.138.01.06
408	Harley SL (1998b) An appraisal of peak temperatures and thermal histories in ultrahigh-
409	temperature (UHT) crustal metamorphism: the significance of aluminous orthopyroxene.
410	Mem Natl Inst Polar Res Spec issue 53:49–73
411	Harley SL (2008) Refining the P-T records of UHT crustal metamorphism. J Metamorph Geol
412	26:125–154. doi: 10.1111/j.1525-1314.2008.00765.x
413	Hensen BJ (1972) Phase relations involving pyrope, enstatitess, and sapphiriness in the system
414	MgO-Al ₂ O ₃ -SiO ₂ . In: Carnegie Inst. Wash. Yearbook 71. pp 421–427
415	Hensen BJ, Essene EJ (1971) Stability of Pyrope-Quartz in the System MgO-Al ₂ O ₃ -SiO ₂ .
416	Contrib Mineral Petrol 30:72–83
417	Hermann J (2003) Experimental evidence for diamond-facies metamorphism in the Dora-Maira
418	massif. 70:163–182. doi: 10.1016/S0024-4937(03)00097-5
419	Herzberg CT (1983) The reaction forsterite+cordierite=aluminous orthopyroxene+spinel in the

420	system MgO-Al ₂ O ₃ -SiO ₂ . Contrib Mineral Petrol 84:84–90. doi: 10.1007/BF01132333
421	Holland TJB (1980) The reaction albite = jadeite + quartz determined experimentally in the
422	range 600-1200 °C. Am Mineral 65:129–134
423	Holland TJB, Green ECR, Powell R (2018) Melting of peridotites through to granites: a simple
424	thermodynamic model in the system KNCFMASHTOCr. J Petrol 59:881–900. doi:
425	10.1093/petrology/egy048
426	Holland TJB, Powell R (2011) An improved and extended internally consistent thermodynamic
427	dataset for phases of petrological interest, involving a new equation of state for solids. J
428	Metamorph Geol 29:333–383. doi: 10.1111/j.1525-1314.2010.00923.x
429	Hollis JA, Harley SL (2003) Alumina solubility in orthopyroxene coexisting with sapphirine and
430	quartz. Contrib Mineral Petrol 144:473–483. doi: 10.1007/s00410-002-0412-3
431	Jenkins DM (2011) The transition from blueschist to greenschist facies modeled by the reaction
432	glaucophane + 2 diopside + 2 quartz = tremolite + 2 albite. Contrib Mineral Petrol 162:725–
433	738. doi: 10.1007/s00410-011-0621-8
434	Jenkins DM, Corona J-C (2006) The role of water in the synthesis of glaucophane. Am Mineral
435	91:1055–1068. doi: 10.2138/am.2006.2014
436	Kawasaki T, Osanai Y (2015) Experimental evidence of bulk chemistry constraint on SiO ₂
437	solubility in clinopyroxene at high-pressure conditions. 226:4–16. doi:
438	10.1016/j.lithos.2015.01.025
439	Kelsey DE (2008) On ultrahigh-temperature crustal metamorphism. Gondwana Res 13:1–29. doi
440	10.1016/j.gr.2007.06.001
441	Kelsey DE, Hand M (2015) On ultrahigh temperature crustal metamorphism: Phase equilibria,
442	trace element thermometry, bulk composition, heat sources, timescales and tectonic settings.

443	Geosci Front 6:311–356. doi: 10.1016/j.gsf.2014.09.006
444	Larson AC, Von Dreele RB (2004) General Structure Analysis System (GSAS). Los Alamos
445	Natl Lab Rep LAUR 86–748
446	Lee HY, Ganguly J (1988) Equilibrium compositions of coexisting garnet and orthopyroxene:
447	Experimental determinations in the system FeO-MgO-Al ₂ O ₃ -SiO ₂ , and applications. J
448	Petrol 29:93-113. doi: 10.1093/petrology/29.1.93
449	Levien L, Prewitt CT, Weidner DJ (1980) Structure and elastic properties of quartz at pressure.
450	Am Mineral 65:920–930
451	MacGregor ID (1974) The system MgO-Al ₂ O ₃ -SiO ₂ : solubility of Al ₂ O ₃ in enstatite for spinel
452	and garnet peridotite compositions. Am Mineral 59:110-119
453	Manning CE (2018) Fluids of the Lower Crust: Deep Is Different. Annu Rev Earth Planet Sci
454	46:67–97. doi: 10.1146/annurev-earth-060614-105224
455	Massonne H-J, Schreyer W (1989) Stability field of the high-pressure assemblage talc+ phengite
456	and two new phengite barometers. Eur J Mineral 391–410. doi: 10.1127/ejm/1/3/0391
457	Nakamura D, Banno S (1997) Thermodynamic modelling of sodic pyroxene solid-solution and
458	its application in a garnet-omphacite-kyanite-coesite geothermobarometer for UHP
459	metamorphic rocks. Contrib Mineral Petrol 130:93-102. doi: 10.1007/s004100050352
460	Nestola F, Gatta GD, Ballaran TB (2006) The effect of Ca substitution on the elastic and
461	structural behavior of orthoenstatite. Am Mineral 91:809-815. doi: 10.2138/am.2006.1982
462	Novak GA, Gibbs GV (1971) The crystal chemistry of the silicate garnets. Am Mineral 56:791–
463	825. doi: 10.1180/minmag.1968.036.281.07
464	Perkins D (1983) The stability of Mg-rich garnet in the system CaO-MgO-Al ₂ O ₃ -SiO ₂ at 1000-
465	1300 °C and high pressure. Am Mineral 68:355–364

466	Perkins D, Holland IJB, R. C. Newton (1981) The Al ₂ O ₃ contents of enstatite in equilibrium
467	with garnet in the system MgO-Al ₂ O ₃ -SiO ₂ at 15-40 kbar and 900-1,600 °C. Contrib
468	Mineral Petrol 78:99-109. doi: 10.1007/BF00371147
469	Powell R, T. J. B. Holland, Worley B (1998) Calculating phase diagrams involving solid
470	solutions via non-linear equations, with examples using THERMOCALC. J Metamorph
471	Geol 16:577–588. doi: 10.1111/j.1525-1314.1998.00157.x
472	Proyer A, Dachs E, McCammon C (2004) Pitfalls in geothermobarometry of eclogites: Fe ³⁺ and
473	changes in the mineral chemistry of omphacite at ultrahigh pressures. Contrib Mineral
474	Petrol 147:305-318. doi: 10.1007/s00410-004-0554-6
475	Schertl H-P, Schreyer W, Chopin C (1991) The pyrope-coesite rocks and their country rocks at
476	Parigi, Dora Maira Massif, Western Alps: detailed petrography, mineral chemistry and PT-
477	path. Contrib Mineral Petrol 108:1-21. doi: 10.1007/BF00307322
478	Schroeder-Frerkes F, Woodland AB, Uenver-Thiele L, Klimm K, Knapp N (2016) Ca-Eskola
479	incorporation in clinopyroxene: limitations and petrological implications for eclogites and
480	related rocks. Contrib Mineral Petrol 171:1–18. doi: 10.1007/s00410-016-1311-3
481	Sekine T, Wyllie PJ (1983) Effect of H ₂ O on Liquidus Relationships in MgO-Al ₂ O ₃ -SiO ₂ at 30
482	kilobars. J Geol 91:195–210. doi: 10.1086/628756
483	Sverjensky DA, Harrison B, Azzolini D (2014) Water in the deep Earth: The dielectric constant
484	and the solubilities of quartz and corundum to 60 kb and 1200 °C. Geochim Cosmochim
485	Acta 129:125–145. doi: 10.1016/j.gca.2013.12.019
486	Toby BH (2001) <i>EXPGUI</i> , a graphical user interface for <i>GSAS</i> . J Appl Crystallogr 34:210–213.
487	doi: 10.1107/S0021889801002242
488	Walker D, Carpenter MA, Hitch CM (1990) Some simplifications to multianvil devices for high

489	pressure experiments. Am Mineral 75:1020–1028
490	Wickham H (2016) ggplot2: elegant graphics for data analysis, 2nd edn. Springer International
491	Publishing
492	

Table 1 Phase synthesis conditions and products

Mineral	Bulk composition	P	T	H ₂ O	t	Products and comments
		(GPa)	(°C)	(wt%)	(h)	
Pyrope ^a	$Mg_3Al_2Si_3O_{12}$	2.50(5)	850(10)	4	96	pyrope; two treatments
Al-free Opx	$Mg_2Si_2O_6$	2.50(5)	850(10)	4	48	Opx
medium-Al Opx ^b	$(Mg_{1.8}Al_{0.2})(Si_{1.8}Al_{0.2})O_6$	1.60(5)	1040(10)	4	24	Opx (96%), sapphirine (4%)
high-Al Opx	$(Mg_{1.7}Al_{0.3})(Si_{1.7}Al_{0.3})O_6$	1.60(5)	1450(10)	0	3.5	Opx (92%), sapphirine (8%)
kyantie	Al ₂ SiO ₅	2.00(5)	850(10)	4	40	kyanite
fayalitec ^c	Fe ₂ SiO ₄	0 (vac)	900(10)	0	72	fayalite
ferrosilite ^d	FeSiO ₃	2.00(5)	900(10)	0	42	ferrosilite

Uncertainties in the last digits of pressure (P), temperature (T), and given in parentheses; phase abundance listed in wt% via Rietveld refinement

^aPyrope was made from oxides and 10 wt% of seeds which were made at 2.5 GPa and 1050 °C for 96 hours within two treatments.

^bMedium-Al Opx was made from oxides and 10 wt% of Al-free Opx

^cFayalite was made by placing a mixture of Fe^o, Fe2O3, and SiO2 of fayalite bulk composition into a graphite crucible, sealing this crucible in an evacuated fused-silica tube, and heating at 900°C for 72 h.

^dFerrosilite was made from an appropriate mixture of fayalite and quartz.

Table 2 Unit-cell parameters of synthetic phases listed in Table 1.

Phase	e Unit-cell dimensions and volume						
	a(Å)	b(Å)	c(Å)	α(°)	β(°)	γ(°)	$V(\text{Å}^3)$
Pyrope	11.45(4)	11.45(4)	11.45(4)	90	90	90	1502.6(2)
AF Opx	18.23(4)	8.816(2)	5.177(2)	90	90	90	831.8(4)
MA Opx	18.195(4)	8.743(1)	5.179(1)	90	90	90	824.0(2)
HA Opx	18.176(3)	8.729(1)	5.1803(2)	90	90	90	821.9(2)
kyantie	7.121(1)	7.848(3)	5.571(3)	90.0(3)	101.2(1)	105.96(6)	293.2(2)

Uncertainties in the last digits of unit-cell parameters given in parentheses

AF Al-free, MA medium-Al, HA high-Al

The results are average values from GSAS Rietveld refinements based on three to five powder XRD analysis of starting materials, with quartz ($a_0 = 4.9139$; $c_0 = 5.40595$ Å) as an internal standard for refinement.

 Table 3 Results of selected experimental reversals on reaction (1).

Code ^a	Nominal P	Corrected P	T	t	Products and comments	
	(GPa)	(GPa)	(°C)	(h)		
14, A1	1.60(5)	1.50(5)	940(5)	72	Opx growth	
15, A2	1.60(5)	1.50(5)	980(5)	72	Opx growth	
16, A3	1.60(5)	1.50(5)	1020(5)	72	Opx growth	
17, A4	1.60(5)	1.50(5)	1040(5)	72	Opx growth	
19, A5, A33	1.60(5)	1.50(5)	1060(5)	24	Unclear ^b	
A34, A36						
49, <i>A30</i>	1.60(5)	1.50(5)	1080(5)	24	Pyrope growth	
A37	1.65(5)	1.55(5)	1080(5)	24	Pyrope growth	
50	1.70(5)	1.60(5)	1100(5)	24	Pyrope growth	
48, <i>A29</i>	1.80(5)	1.69(5)	1000(5)	24	Opx growth	
23, A9	1.80(5)	1.69(5)	1100(5)	24	Pyrope growth	
46, <i>A26</i>	1.90(5)	1.79(5)	1000(5)	24	Pyrope growth	
3	2.00(5)	1.88(5)	820(5)	72	Opx growth	
1	2.00(5)	1.88(5)	860(5)	48	Opx growth	
25, <i>A24</i>	2.00(5)	1.88(5)	1000(5)	24	Pyrope growth	
27, A13	2.10(5)	1.97(5)	1000(5)	24	Pyrope growth	
26, A12	2.20(5)	2.07(5)	1000(5)	24	Pyrope growth	
28, A14	2.40(5)	2.26(5)	900(5)	24	Opx growth	
31, A17, <i>A25</i>	2.40(5)	2.26(5)	920(5)	24	Opx growth	
6	2.40(5)	2.26(5)	820(5)	48	Opx growth	

7	2.40(5)	2.26(5)	840(5)	48	Opx growth
30, A16	2.40(5)	2.26(5)	940(5)	24	Pyrope growth
29, A15	2.50(5)	2.35(5)	900(5)	24	Opx growth
34, <i>A22</i>	2.90(10)	N. A.	820(10)	48	Opx growth
53, A35, <i>A28</i>	2.90(10)	N. A.	840(10)	48	Opx growth
32	2.90(10)	N. A.	860(10)	48	Pyrope growth
55	2.90(10)	N. A.	880(10)	48	Pyrope growth
36	3.30 (10)	N. A.	780(10)	24	Pyrope growth
38	3.30 (10)	N. A.	760(10)	48	Talc nucleation
37	3.30 (10)	N. A.	740(10)	48	Talc nucleation

Uncertainties in the last digits of pressure (P), temperature (T), and given in parentheses.

N.A. not applicable.

^aMultiple runs were conducted at most P-T conditions with different starting materials, especially those near the reaction boundary. The number code (XX) indicates Al-free Opx. The AX code indicates medium-Al Opx, while the italic AX indicates high-Al Opx.

^bFive runs were conducted at this condition, but contradictory results were produced (3 for Opx growth but 2 for pyrope growth), which may indicate a condition very near to the reaction boundary.

Table 4 Average composition of run-product orthopyroxene measured from electron microprobe and unit-cell parameters derived from Rietveld structure refinements.

code	Average values			Unit-cell parameters of Opx ^a						
code	Al/6 O	X _{En}	$X_{ m MgTs}$	$X_{ m MgEs}$		<i>a</i> (Å)	<i>b</i> (Å)	c (Å)	$V(\text{Å}^3)$	V _m (J/bar) ^b
19	0.37	0.78	0.15	0.08		18.191	8.736	5.176	822.623	6.192(195)
A33	0.40	0.76	0.17	0.07		18.192	8.737	5.178	822.985	6.195(186)
A36	0.49	0.71	0.20	0.10		18.176	8.724	5.177	820.932	6.180(185)
48	0.30	0.80	0.10	0.09		18.161	8.743	5.170	820.885	6.179(171)
A29	0.47	0.72	0.19	0.09		18.185	8.737	5.179	822.892	6.194(227)
31	0.12	0.91	0.02	0.07		18.216	8.798	5.175	829.413	6.243(235)
A17	0.36	0.78	0.14	0.08		18.193	8.751	5.178	824.332	6.205(138)
A25	0.42	0.73	0.15	0.11		18.182	8.746	5.178	823.302	6.197(209)
53	0.15	0.88	0.03	0.10		18.221	8.803	5.180	830.853	6.254(316)
A35	0.38	0.77	0.15	0.08		18.201	8.765	5.177	825.956	6.217(171)
A28	0.43	0.73	0.16	0.10		18.212	8.759	5.177	825.798	6.216(382)
34	0.13	0.9	0.04	0.06		18.213	8.799	5.178	829.787	6.246(246)
A15	0.35	0.77	0.12	0.11		18.191	8.756	5.177	824.618	6.207(140)

Uncertainties in the last digits of unit-cell volumes are given in parentheses, while typical values with uncertainties of X_{MgTs} and X_{MgEs} are shown in Figure 6.

^aQuartz was used as the internal standard, with $a_0 = 4.9139$ Å and $c_0 = 5.40595$ Å.

^bThe molar volume $V_{\rm m}$ (J/bar) = $V_{\rm cell}$ (Å) \cdot 10⁻³⁰ \cdot N_A \cdot 10⁵/ Z = 0.0075 \cdot $V_{\rm cell}$ (Å³), where N_A represents the Avogadro constant, and Z, the number of formula units per unit cell for orthopyroxene, is 8.

Figure Captions

Figure 1 a Schematic diagram of the double-sleeve NaCl-pyrex pressure cell for the ½ inch diameter piston cylinder. **b** Powder XRD patterns showing the progressive development of ferrosilite against fayalite + quartz with increasing pressure from the starting mixture at 1000 °C, used to calibrate the sample pressure for the assemblage.

Figure 2 Reversal experiments for reaction (1). Open circles represent growth of orthopyroxene, while solid circles represent growth of pyrope. Half-filled circle represents no clear reaction, and squares represent the nucleation of talc. Most experiments were repeated with 1-3 different starting materials, especially those near to the boundary. The dashed line represents the modeled boundary based on the binary enstatite—MgTs solution model of orthopyroxene from Holland et al. (2018), while the dotted line represents the uncorrected "piston out" reversal bracket of Hensen (1972). The quartz-coesite boundary is that of Bose and Ganguly (1995) which is adopted by Holland and Powell (2011).

Figure 3 Compositional reversals in the Al_2O_3 contents (wt%) of orthopyroxene in starting materials and run products near the reaction boundary. Ranges bounded by arrows indicate the interpreted Al_2O_3 contents of orthopyroxene at equilibrium. Note that the values are not mean and standard deviations but are based on the extent of compositional overlap from different starting composions as well as the population of Al_2O_3 contents observed (see text).

Figure 4 En-MgTs-MgEs ternary diagrams showing the mole fraction of the three components of orthopyroxene under different *P-T* conditions: (a) starting orthopyroxene, (b) 1.50 GPa and

1060 °C, (c) 1.69 GPa and 1000 °C, (d) 2.26 GPa and 920 °C, and (e) 2.90 GPa and 840 °C. The ternary diagrams have been drawn using packages ggplot2 and ggtern in R (Wickham 2016; Hamilton and Ferry 2018).

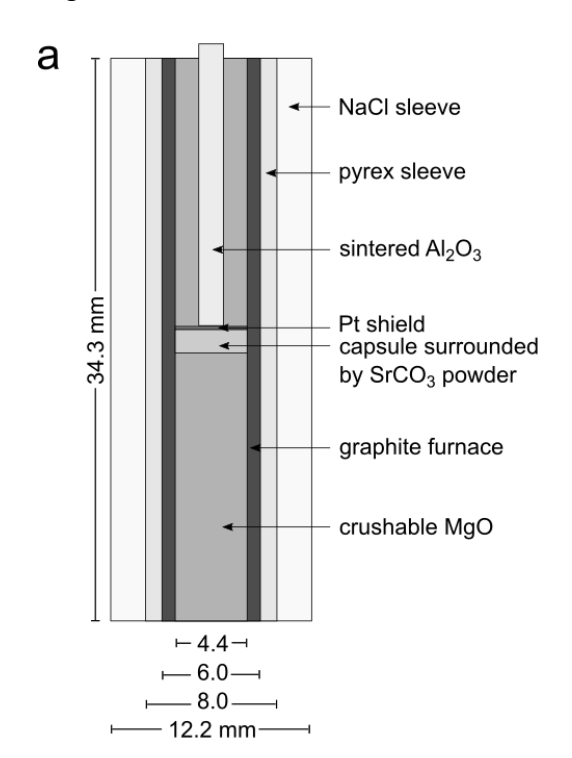
Figure 5 X_{MgEs} V_{MgEs} X_{MgEs} diagram showing the linear derivation of the molar volume of MgEs as discussed in the text. The data are from this study and Fockenberg and Schreyer (1997).

Figure 6 *P-T* diagram showing calculated cures with and without MgEs, and the experimental brackets. The upper values indicate average and standard deviation of the mole fraction of MgTs (X_{MgTs}) , and the lower values indicate those of MgEs (X_{MgEs}) , respectively, based on the interpreted ranges in Figure 3.

Figure 7 *P-T* diagram showing the Si-in-phengite barometer with Si = 3.55 and reactions Opx + kyanite = pyrope + coesite and talc + kyanite = pyrope + coesite + H₂O. The Si-in-phengite barometer is from Massonne and Schreyer (1989) and Si = 3.55 in phengite (dashed line) is according to Schertl et al. (1991). The Opx + kyanite reaction (black line) is calculated using the new model for orthopyroxene from this study. The talc + kyanite reaction (grey line) is calculated based on the activity model of Holland et al. (2018) assuming a_{H_2O} =1. The experimental constraint for the talc + kyanite reaction is from Chopin (1985) in which the solid circle represents decline of talc + kyanite, open circles growth of talc + kyanite, and half-circles represent no obvious reaction.

Figure 8 Calculated P-T diagram showing the Al_2O_3 isopleths (dashed lines) in orthopyroxene in the MAS assemblage orthopyroxene + sapphirine (Sa) + quartz (Qz), with MgEs and without MgEs. The upper and lower boundaries are the reactions Opx + sillimanite (sill) = sapphirine + quartz and cordierite (Crd) = sapphirine + Opx + quartz, respectively. Numbers indicate total Al_2O_3 wt% content in Opx.

Figure 1



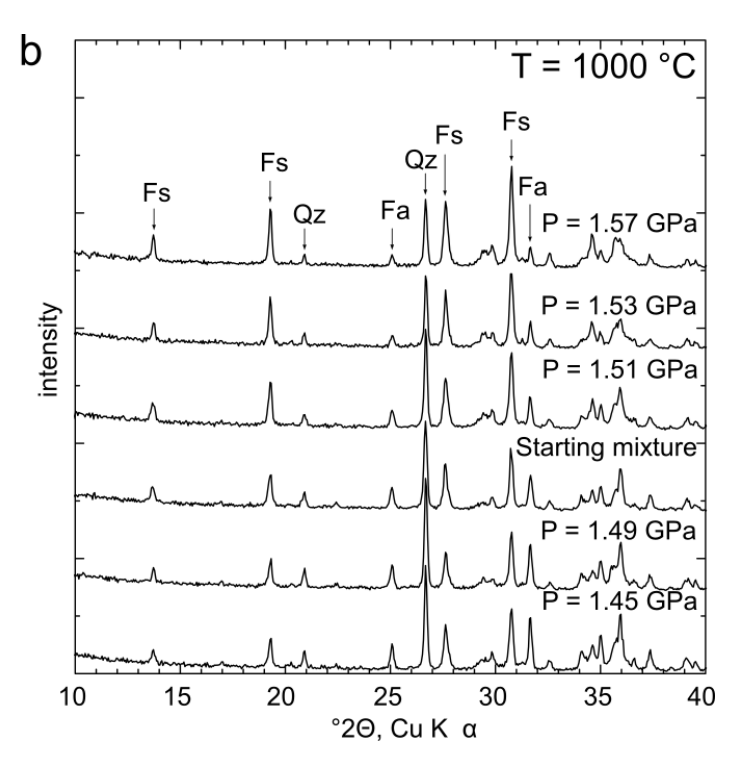


Figure 2

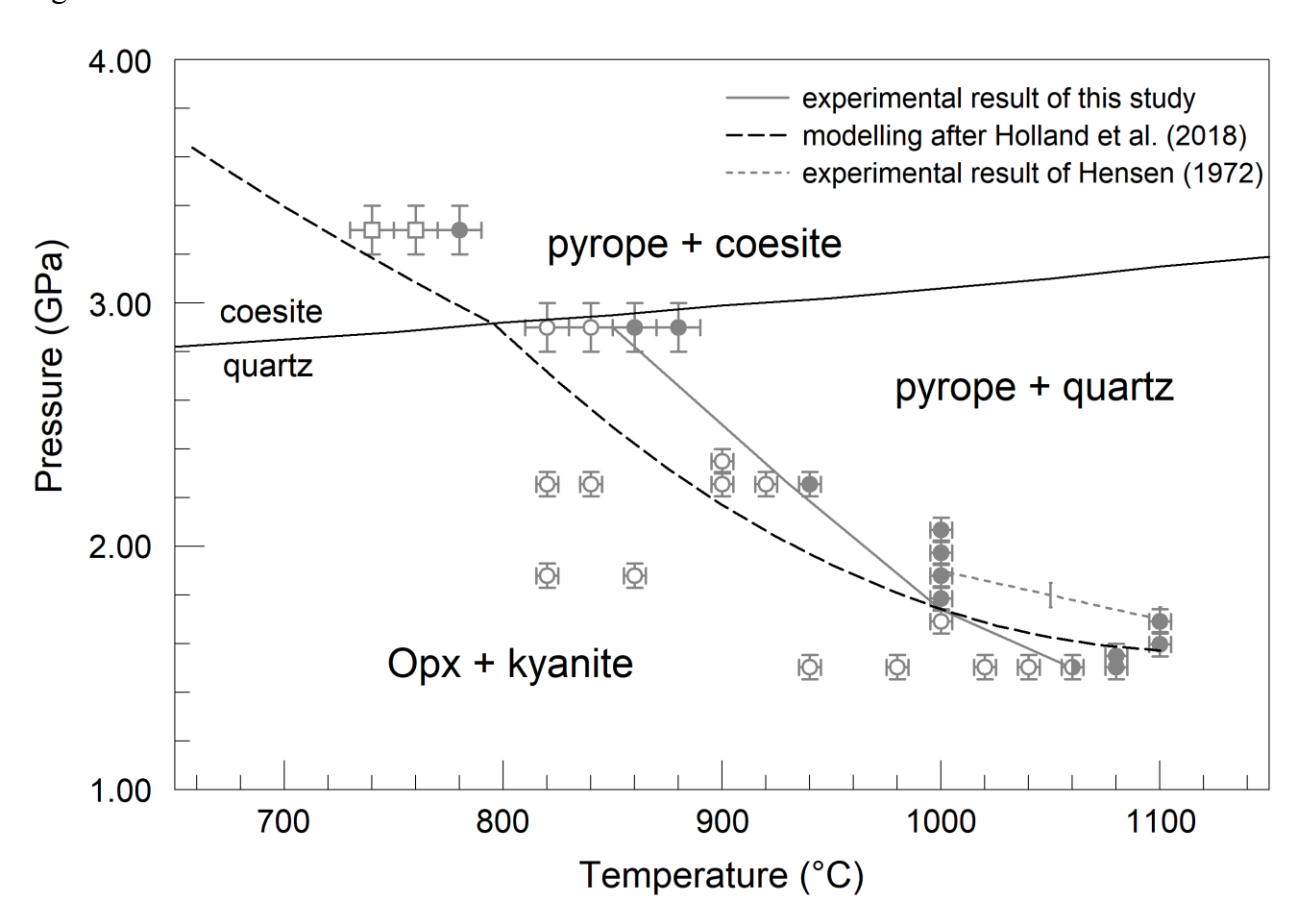


Figure 3

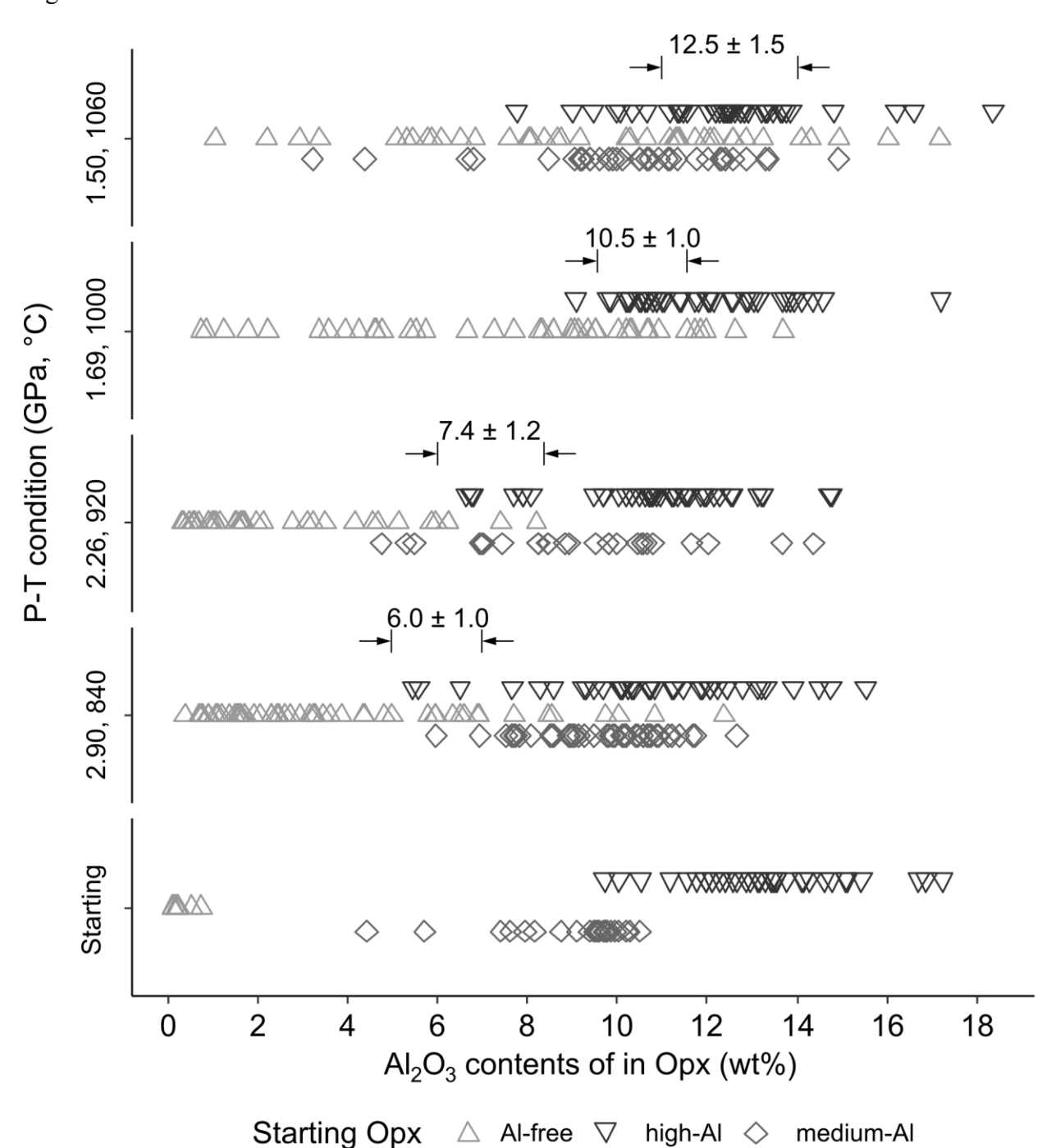


Figure 4

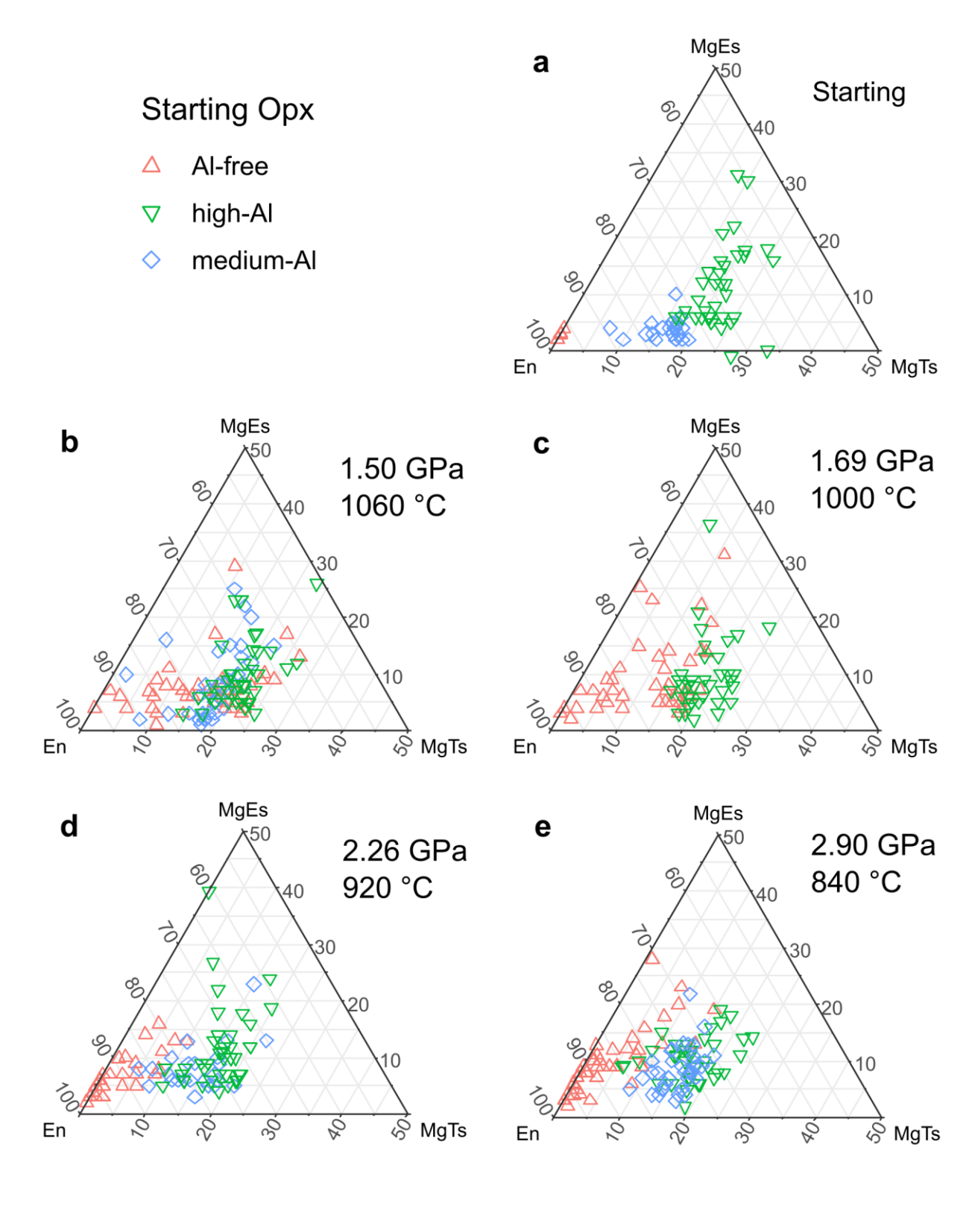


Figure 5

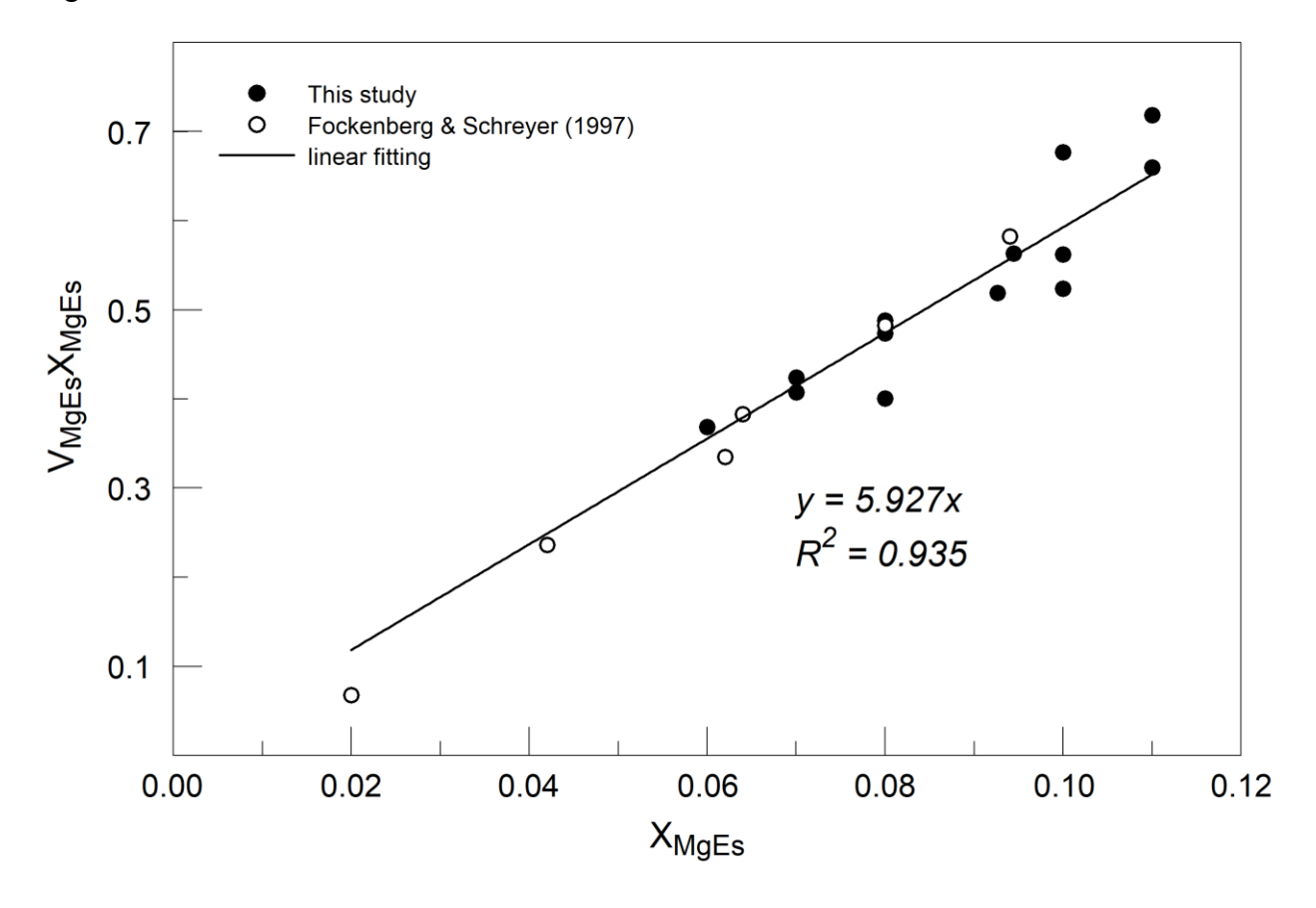


Figure 6

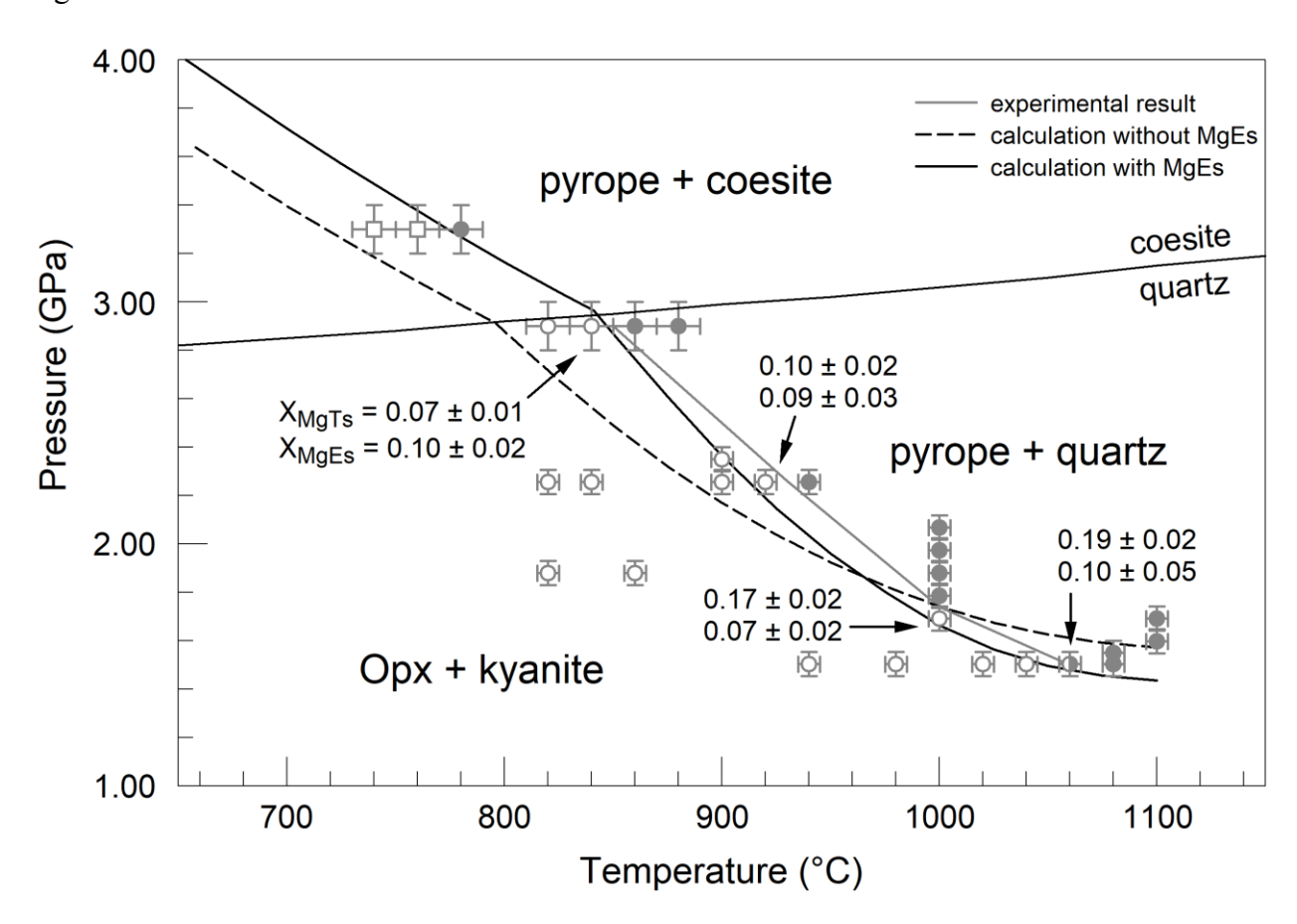


Figure 7

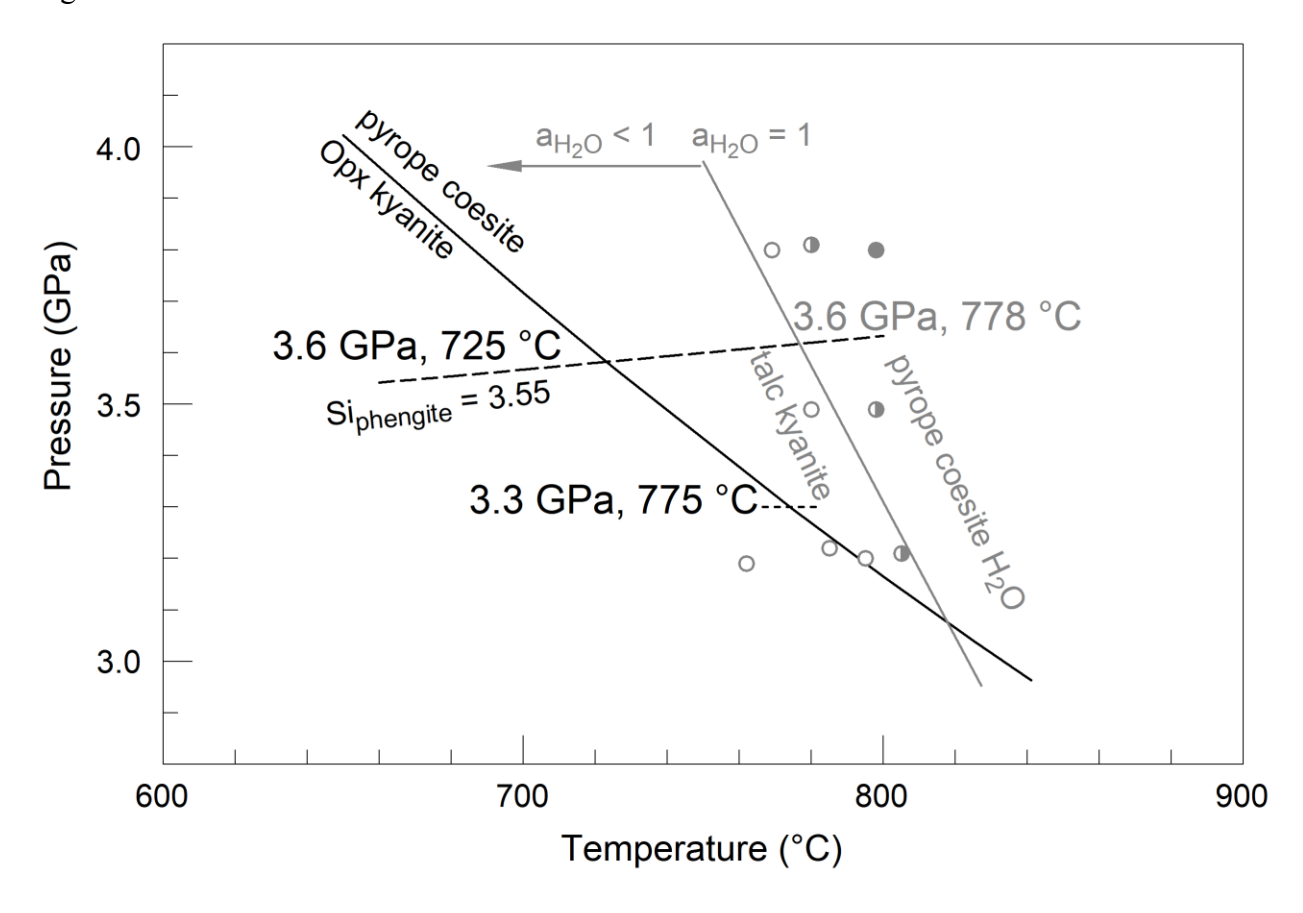


Figure 8

